Observations for Chemistry (Remote Sensing): Microwave (Ground, Aircraft, Balloon, Satellite)

Joe Waters
California Institute of Technology Jet Propulsion Laboratory
Pasadena, California 91109, USA

manuscript no. 271 to be published in
Academic Press Ltd
Encyclopedia of Atmospheric Sciences
edited by Jim Holton, Judy Curry and John Pyle

contents

Introduction

Microwave remote sensing observations for atmospheric chemistry have been obtained from ground, aircraft, balloon and satellite platforms. Examples of results are given later in this article, after describing the measurement fundamentals, chemical species having microwave spectra, and instrumentation. The technique has been used, to date, for observations of stratospheric and mesospheric chemistry. It has not yet been applied to tropospheric chemistry - primarily because of difficulties associated with (1) tropospheric H_2O absorption and (2) the larger widths of tropospheric spectral lines. Recent technology advances have removed difficulty (2), and future application to the *upper* troposphere, where there are sufficient spectral windows, is expected. Microwave observations of chemical species can be made in the presence of clouds and volcanic aerosols that limit shorter-wavelength infrared, visible and ultraviolet techniques.

'Microwave' is used here to denote heterodyne measurements at centimeter, millimeter and submillimeter wavelengths. The spectral range of interest extends, roughly, from the 1.35 cm wavelength (22 GHz frequency, 1 GHz = 10^9 Hz) H_2O spectral line through the 0.12 mm wavelength (2.5 THz frequency, 1 THz = 10^{12} Hz) OH lines. 'Heterodyne' indicates multiplying a weak input signal by a strong local oscillator signal to translate - without loss of information - the input signal to a portion of the spectrum more convenient for further processing. This process allows measurements of weaker signals, and better spectral resolution, than generally can be obtained with other techniques. Technology for low-noise submillimeter heterodyne measurements has become available only recently, and is advancing rapidly. Far-infrared non-heterodyne techniques made the first measurements of the atmospheric submillimeter spectrum.

Resolved spectral lines, providing unique signatures of selected species, are generally measured. Measurements can be either of atmospheric thermal emission or of absorption against a source such as the sun; most are of thermal emission in order to obtain results at all times of day and night. Temperature is typically obtained from emission by O_2, but can also be obtained from other gases. The rotational states usually sensed are in thermal equilibrium well up through the mesosphere, easing interpretation. The relatively-weak (approximately-linear) temperature-dependence of the Planck function, at the observed wavelengths and temperatures, means that

uncertainties in atmospheric temperature generally do not limit accuracy of the measured abundance. The resolved line measurements give robust results by allowing differences to be taken between outputs from nearby channels 'on' and 'off' a line; this can eliminate artifacts while retaining the signal. The 'shape' of output from channels covering the line, which must have a certain form, also provides robustness and information on the altitude profile. Mathematical techniques for retrieving abundance and temperature from the measurements are well established.

Fig. 1 shows the tropospheric spectrum for the wavelength region considered here. The window at ~200-300 GHz is especially productive for ground-based measurements of stratospheric chemistry. Aircraft, balloon, and satellite platforms usually must be employed for measurements above ~300 GHz due to tropospheric H_2O absorption.

<insert Figure 1 near here>

Measurement Fundamentals

The power in the atmospheric signal measured at frequency ν over incremental range $d\nu$ can be written

$$dP_\nu = \frac{1}{2} d\nu \int_\Omega I_\nu(\theta,\phi) A_e(\theta,\phi) d\Omega \quad , \qquad [1]$$

where $I_\nu(\theta,\phi)$ is the intensity [W Hz^{-1} m^{-2} sr^{-1}] of atmospheric radiation from direction (θ,ϕ) and $A_e(\theta,\phi)$ is the instrument's effective collecting area in that direction. The integration is over all solid angle Ω ; ½ appears because only one polarization is received and random polarization is assumed here for the atmospheric radiation. The collecting area of a heterodyne 'radiometer' (instrument for measuring radiative power) has the property

$$\int_\Omega A_e(\theta,\phi)\, d\Omega \;=\; \lambda^2 \quad , \qquad [2]$$

where $\lambda = c/\nu$ is the wavelength of the radiation ($c = 2.998\times10^8$ m/s is the speed of light), and is related to $G(\theta,\phi)$, the instrument's 'antenna gain pattern', by $A_e(\theta,\phi) = \lambda^2\, G(\theta,\phi) / 4\pi$.

Equation [2] has important practical implications: the instrument's collecting area integrated over solid angle is just the square of the wavelength, independent of its 'physical' size. The power

collected from a source that fills the antenna beam, generally true for atmospheric measurements, is *not* increased by increasing the physical size of the aperture for a *heterodyne* instrument. The increase in power that might have been expected from the aperture size increase is, due to diffraction effects, offset by a decrease in the angular range over which radiation is collected. The instrument field-of-view (FOV) width [in radians] in a particular plane is, approximately, the inverse of the aperture dimension [in wavelengths] in that plane. Because the integrated collecting area is λ^2, the power per unit frequency interval collected at frequency ν from blackbody radiation is $\frac{1}{2}\lambda^2 B_\nu(T)$, where $B_\nu(T) = (2h\nu^3/c^2)/(e^{h\nu/kT} - 1)$ is Planck's function giving the radiation intensity; $h = 6.626\times10^{-34}$ J s is Planck's constant, $k = 1.38\times10^{-23}$ W Hz^{-1} K^{-1} is Boltzmann's constant. For temperatures in Earth's atmosphere, $\frac{1}{2}\lambda^2 B_\nu(T)$ is nearly constant with ν up to ~5 THz, beyond which it drops rapidly, as shown in **Fig. 2.** Heterodyne measurements of atmospheric thermal emission are, thus, relatively efficient at frequencies up to ~5 THz ($\lambda >$ ~6×10^{-5} m) but not much beyond. Shorter wavelength (e.g., infrared) heterodyne atmospheric measurements are usually made of solar absorption.

<insert Figure 2 near here>

The intensity of radiation from a specified direction is given by the radiative transfer equation

$$I_\nu = I_\nu(0)\, e^{-\tau(0,L)} + \int_0^{\tau_\nu(0,L)} B_\nu(T)\, e^{-\tau_\nu(s,L)}\, d\tau_\nu(s) \quad , \qquad [3]$$

where the integral is over the radiation path through the atmosphere, the instrument is at L, $I_\nu(0)$ is the radiation at point *0* outside the atmosphere, and

$$\tau_\nu(s,L) = \int_s^L \alpha_\nu(s)\, ds \qquad [4]$$

is the 'optical depth' at frequency ν between points s and L on the path where $\alpha_\nu(s)$ is the 'absorption coefficient' (having dimension 1/length) at s. Combining [1] - [3], the power collected from a thermal emission signal (no $I_\nu(0)$ term in [3]) over frequency range $\Delta\nu$ can be written

$$P_{sig} = \frac{\lambda^2}{2}\,\overline{B_\nu(T)}\cdot(1-e^{-\tau_\nu(0,L)})\cdot\Delta\nu \quad \overset{\tau_\nu(0,L)\ll 1}{\rightarrow} \quad \frac{\lambda^2}{2}\,\overline{B_\nu(T)}\cdot\tau_\nu(0,L)\cdot\Delta\nu \qquad [5]$$

where the fact that $B_\nu(T)$ is a relatively weak function of $\tau_\nu(s)$ allows appropriate means (indicated by an overbar) to be taken outside the integrals in [3] and [1], and the rightmost expression in [5] applies to signals with small optical depth. The microwave signal power is usually expressed as signal 'brightness temperature'. This quantity is proportional to the detected power from the signal, has units of temperature, and for $h\nu << kT$ converges to the temperature of blackbody radiation that would give rise to the amount of detected power from the signal:

$$T_{sig} \equiv \frac{P_{sig}}{k\,\Delta\nu} \quad \overset{\tau_\nu(0,L) >> 1}{\rightarrow} \quad \frac{\lambda^2}{2\,k}\,\overline{B_\nu(T)} \quad \overset{h\nu << kT}{\rightarrow} \quad \overline{T}\,, \qquad [6]$$

where [5] has been used to obtain the expression for large optical depth after the first arrow in [6].

The absorption coefficient for an isolated spectral line is given by

$$\alpha_\nu^{ul} \;=\; n\,\frac{2\pi^2\, g_l\, g_u\, \phi_{ul}^2\, \mu^2}{3\,\varepsilon_o\, hc\; Q(T)}\left[e^{-E_l/kT} \;-\; e^{-E_u/kT}\right]\cdot \nu \cdot b(\nu,\nu_{ul})\,, \qquad [7]$$

where n is number density of the species with the spectral line, u and l denote the upper and lower quantum states involved in the transition, g_l is the degeneracy and E_l the energy for state l, ϕ_{ul}^2 is the transition matrix element (sometimes g_u is included in ϕ_{ul}^2), μ is the overall dipole (or other) moment coupling to the radiation field, and $\varepsilon_o = 8.854\times10^{-12}$ F m^{-1} is the permittivity of vacuum. $Q(T)=\Sigma g_l \exp(-E_l/kT)$ is the partition function, and it is assumed that the quantum states are in thermal equilibrium at temperature T. The 'line shape function' $b(\nu, \nu_{ul})$, normalized such that $\int b(\nu, \nu_{ul})\, d\nu = 1$, gives the probability density that the transition is observed at frequency ν rather than the nominal $\nu_{ul} = (E_u - E_l)/h$.

Atmospheric microwave line shapes are dominated by collision (pressure) broadening at lower altitudes and Doppler (thermal motion) broadening at higher altitudes. The collision linewidth parameter (half width at half maximum) can be written $\Delta\nu_c^{ul} = (\Delta\nu_{co}^{ul})\cdot(p/1\text{ hPa})\cdot(T/300\text{ K})^{-x}$ where p is atmospheric pressure, $\Delta\nu_{co}^{ul}$ and x are constants. Typical values are $\Delta\nu_{co}^{ul} = 2.5$ MHz, $x = 0.75$. The Lorentz shape, $b(\nu, \nu_{ul}) = [\Delta\nu_c^{ul}/\pi] / [(\nu - \nu_{ul})^2 + (\Delta\nu_c^{ul})^2]$, is applicable to narrow collision-broadened lines measured for atmospheric chemistry. Doppler broadening gives a Gaussian shape $b(\nu, \nu_{ul}) = (1/\Delta\nu_D^{ul})\,(\ln 2 / \pi)^{1/2} \exp\{-\ln 2\,[(\nu - \nu_{ul})/(\Delta\nu_D^{ul})]^2\}$ with linewidth parameter $\Delta\nu_D^{ul} = (\nu_{ul}/c)\cdot(2\ln 2\; kT/m)^{1/2} = 3.58\times10^{-7}\cdot\nu_{ul}\cdot(T/m)^{1/2}$, where m is the molecular mass

in grams/mole and T is in K. The Voigt shape (convolution of collision and Doppler shapes) applies when both Doppler and collision broadening are important. **Fig. 3** shows representative linewidths versus altitude. The collision linewidth for O_2 is noticeably smaller than the others in Fig. 3 because collision linewidths generally increase with dipole moment and O_2 has a very small (magnetic) one. Doppler broadening is important above ~80 km for the 22 GHz H_2O line, decreasing to ~40 km for the 2.5 THz OH line.

<insert Figure 3 near here>

The line shape function at the center of a collision-broadened line has value $1/(\pi \Delta\nu_c^{ul})$. Equation [7] then becomes

$$\alpha_{\nu_{ul}}^{ul} = \frac{f \mu^2}{Q(T)} S_{ul}(T) \qquad [8]$$

where $f \equiv n/N$ is the volume mixing ratio of the gas whose spectral line is being measured, N being atmospheric total number density, $\Delta\nu_c^{ul} \propto p\, T^{-x} \propto N\, T^{1-x}$ has been used, and all transition and frequency-dependent terms, and constants, are placed in $S_{ul}(T)$. Equation [8] shows that the intensity at center of a (small optical depth) collision-broadened line is proportional to volume mixing ratio of the species. **Fig. 4** shows a spectral line for the same mixing ratio at the top, middle and bottom of the stratosphere.

<insert Figure 4 near here>

Chemical Species and Spectra

Many chemical species have spectral lines in the wavelength region considered here. It is useful to have a 'figure of merit' that, in some sense, indicates the typical strength of a microwave spectral line from a particular species and can provide a first step for exploring measurement feasibility. Extracting factors from Equation [8] that depend only upon the species' overall properties yields $M = f\mu^2/Q$ as a 'figure of merit'. Abundance of the species is described by f, μ^2 describes its overall interaction strength with radiation, and Q roughly indicates the number of

quantum states over which it is spread. **Table 1** lists stratospheric species in order of decreasing *M* for approximate maximum abundances in the stratosphere. Symmetric molecules (e.g., CH_4 and CO_2) with no dipole moment and no microwave spectra are missing, as are complex molecules (e.g., chlorofluorocarbons) having large partition functions that cause their 'figures of merit' to be lower than those included in the table. Examination of a species' spectrum, and - to avoid interference - the spectra of other species having *M* greater than ~10× below that of the targeted species, is required to determine measurement feasibility and the spectral line(s) best suited. A catalog maintained by the Molecular Spectroscopy Group at the California Institute of Technology Jet Propulsion Laboratory (see world wide web site http://spec.jpl.nasa.gov) has microwave line parameters for the species in Table 1, and many more. Line frequencies are typically known to ~0.1 MHz or better; strengths to ~1% or better. Dipole (and other) moments are measured from Stark and Zeeman splitting of spectral lines, allowing line strengths to be determined without requiring measurement of the gas abundance in a laboratory cell. Linewidth parameters can be measured with ~3% accuracy.

<insert Table 1 near here>

Fig. 5 shows, on a very compressed scale, representative spectra including those of radicals involved in the major chemical cycles for stratospheric ozone destruction. **Fig. 6** shows an expanded region near 625 and 650 GHz where the strongest rotational line of ClO and the first rotational line of HCl occur.

<insert Figure 5 near here>

<insert Figure 6 near here>

Instrumentation

Fig. 7 gives a typical block diagram of a microwave instrument for atmospheric chemistry observations. Atmospheric signals are collected by an antenna, possibly amplified or filtered, and passed to a mixer. The mixer combines the atmospheric signal with a monochromatic local oscillator (LO) signal in a non-linear process that reproduces the signal spectra at frequencies that are sums and differences of the atmospheric and LO signal frequencies, and possibly at their

harmonics. State-of-the-art mixers are based on planar Schottky-diodes (either cooled or room temperature), superconductor-insulator-superconductor (SIS) tunnel junctions, or superconducting hot electron bolometer (HEB) devices. The LO frequency is chosen so the mixing product of interest (usually at the difference between the LO and signal frequencies) appears at intermediate frequencies (IF) convenient for further processing. The IF signal, after amplification, is passed to a spectrometer that separates it into individual spectral channels with desired resolution. Each channel's signal is then 'detected' (converted to a voltage proportional to its power), digitized and passed to the data handling system. Instruments often contain multiple mixers, LOs, IF amplifiers and spectrometers to allow simultaneous observations of several spectral lines. LO frequencies can be changed operationally to change measurements. Radiometers can be 'chopped', to reduce amplifier gain variation effects, by rapidly moving a 'reference' target in and out of the signal path or by frequency-switching the LO. An instrument sufficiently stable between calibrations does not require chopping and has twice the sensitivity of an otherwise-identical symmetrically-chopped instrument.

Calibration is performed by inserting targets (typically blackbody targets - with 'cold space' generally used for one target when possible) in the signal path near the instrument input, ideally before the antenna. 'Double sideband' (DSB) radiometers receive signals in two mixer 'sidebands', at IFs above and below the LO, whereas 'single sideband' (SSB) radiometers receive signals in only one sideband. The DSB thermal calibration signal, coming through both sidebands, is twice that for SSB. A spectral line occurring in only one sideband appears half as strong when (thermally) calibrated DSB as when calibrated SSB. Accurate calibration can require measuring and accounting for the responses in the two sidebands.

The sensitivity of a microwave radiometer is usually specified by its 'receiver noise temperature', a quantity that is proportional to the instrument noise power referenced to the instrument input. The root mean square measurement noise, expressed in temperature units, for integration time Δt and spectral resolution $\Delta \nu$ is given by

$$\Delta T_{rms} \approx a \cdot \frac{T_{rec} + T_{sig}}{\sqrt{\Delta t \cdot \Delta \nu}} \qquad [9]$$

where T_{rec} is the receiver noise temperature, and $a \approx 1$ for a non-chopped system or $a \approx 2$ for a chopped system. T_{sig}, usually much smaller than T_{rec} for thermal emission measurements, is present

because the signal itself is noisy. The value of T_{rec} is primarily set by noise in the first amplifier and the amount of signal loss preceding it. Advances in technology are rapidly reducing noise and extending spectral bandwidth. Current state-of-the-art values of T_{rec} (SSB values, or 2×DSB values) for the ~200-300 GHz range with ~0.5 GHz bandwidth are ~2000 K for room temperature radiometers and ~400 K for SIS radiometers. Bandwidth can be increased at the cost of somewhat increased noise: room temperature radiometers at ~200 GHz have been developed with $T_{rec} \approx 4000$ K and ~15 GHz IF bandwidth. The measurement noise with $\Delta\nu$=16 MHz resolution and Δt=1 s integration, for example, is $\Delta T_{rms} \approx 1$ K for $T_{rec} \approx 4000$ K and $\Delta T_{rms} \approx 0.1$ K for $T_{rec} \approx 400$ K. Increasing the integration time to 1 hour gives $\Delta T_{rms} \approx 0.02$ K for $T_{rec} \approx 4000$ K and $\Delta T_{rms} \approx 0.002$ K for $T_{rec} \approx 400$ K. Microwave radiometer noise generally increases with frequency, but this can be offset by increases in line strength. A 22 GHz radiometer for ground-based stratospheric H_2O measurement (T_{sig} ~0.2 K) has $T_{rec} \approx 100$ K with ~0.5 GHz bandwidth and 20 K cooled first-stage transistor amplifier. A 2.5 THz room temperature radiometer with ~15 GHz IF bandwidth developed for satellite OH measurements (T_{sig} ~100 K for mid-upper stratospheric OH) has $T_{rec} \approx$ 20,000 K. HEB radiometers at 2.5 THz have been constructed recently with $T_{rec} \approx 3000$ K and ~10 GHz bandwidth; improvements are expected as this technology matures.

Several types of spectrometers are currently used. Filter banks have a set of simultaneously-observed spectral filters, usually made of discrete or distributed capacitative and inductive elements, whose frequencies and widths are set as needed for a particular measurement. Digital autocorrelators measure a signal's autocorrelation simultaneously at many time lags; Fourier transforming the measured autocorrelation function gives the spectrum. Acousto-optic spectrometers use the IF signal to modulate a Bragg cell which, according to the signal's spectral content, diffracts a laser beam to a detector array. Chirp transform spectrometers multiply the IF signal by a frequency-modulated (chirp) waveform, convolve the resulting product with a filter that is appropriately matched to the chirp, and the spectrum appears as a function of time at the output.

Ground-based Observations

Ground-based observations can provide continuous monitoring at selected sites. Instrumentation can be upgraded and repaired if needed, and can rapidly respond to changing priorities and atmospheric conditions. Vertical resolution is obtained from the spectral line shape, and is typically around one atmospheric pressure scale height (~6-8 km) but can be somewhat smaller with good signal to noise. Initial ground-based microwave measurements in the 1970s included stratospheric and mesospheric O_3 from lines near 100 GHz, and high-rotational lines of O_2 (on the edge of its 60 GHz spin-rotation band) that are very sensitive to stratospheric temperatures. Mesospheric CO was first measured by 115 GHz ground-based observations, with many later measurements at 230 GHz. Early measurements of the 22 GHz H_2O line showed a dry stratosphere - in contrast to many previous balloon *in situ* measurements (now thought to have been contaminated) that indicated a very wet stratosphere.

Ground-based microwave measurements have provided important results for understanding stratospheric chlorine chemistry. In 1981 they gave the first definitive remote measurements of ClO, the key chlorine radical involved in ozone depletion. Early results also included the first measurement of ClO diurnal variation, testing crucial aspects of upper stratospheric chlorine chemistry. In 1986 the technique gave the first evidence of greatly enhanced ClO in the Antarctic lower stratosphere, firmly connecting chlorine chemistry to the ozone hole. **Fig. 8** shows an example of ClO evolution observed over Antarctica. Measurements of ClO diurnal variation tested chemical models for formation and photolysis of the ClO dimer in the Antarctic lower stratosphere. Enhanced ClO in the Arctic winter stratosphere also has been measured. HNO_3 - important in processes involving polar stratospheric clouds (PSCs) and quenching of reactive chlorine - has been measured, as has N_2O which gives information on dynamics.

<insert Figure 8 near here>

Additional results include measurement of stratospheric HCN, and studies of mesospheric HO_x chemistry from measurements of HO_2, O_3 and H_2O. The O_2 $^1\Delta_g$ excited electronic state in the mesosphere has been measured, including diurnal variation, and implications obtained for its

radiative lifetime and chemistry. Zeeman splitting of mesospheric O_2 lines has been measured. The 250 GHz line from thermospheric NO has been measured. Ground-based microwave instruments are currently used by several research groups, and are deployed in the international Network for the Detection of Stratospheric Change to measure stratospheric ClO, O_3 and H_2O.

Aircraft-based Observations

Aircraft-based observations can provide measurements with good horizontal resolution along a measurement track over an extended spatial range. Instruments can observe in high-frequency spectral windows where tropospheric H_2O absorption (Fig. 1) prevents ground-based measurements and where more species have spectral lines. Vertical resolution is obtained from spectral line shape for measurements above the aircraft altitude, and can be obtained from limb sounding techniques at heights below the aircraft. Initial aircraft measurements in the 1970s included stratospheric H_2O and O_3 from lines near 183 GHz, and an upper limit on stratospheric ClO abundance. Recent measurements include stratospheric HCl, ClO, O_3, HNO_3, N_2O, H_2O, HO_2, BrO and volcanic SO_2 from a 600 GHz SIS radiometer. **Fig. 9** shows HCl and ClO results from a flight through the edge of the Arctic vortex. OH and H_2O have been measured from aircraft with a room-temperature 2.5 THz radiometer.

<insert Figure 9 near here>

Balloon-based Observations

Balloon-based microwave observations can provide measurements throughout the stratosphere with 2-3 km vertical resolution. The instrument FOV is vertically-scanned through the atmospheric limb to observe a long path length and to obtain the vertical resolution. Balloon instruments provide measurements to higher altitudes with better resolution than can be obtained from aircraft or ground, and provide valuable development and tests of techniques to be deployed on satellites. Initial measurements in the 1980s were of ClO and O_3 from lines near 205 GHz. A 600 GHz room-temperature instrument for measuring HCl, ClO, HNO_3, N_2O, O_3 and HO_2 became operational in the early 1990s; some results are shown in **Fig. 10**. Simultaneous measurement of HCl and ClO gives a stringent monitor of stratospheric chlorine chemistry, and first results from the 600 GHz balloon instrument showed that the ClO/HCl ratio in the midlatitude upper stratosphere could not be explained by chemical models current at the time. Reaction of OH and ClO producing HCl,

hypothesized as cause of the discrepancy, has since been measured in the laboratory with a rate that adequately explains the observations. Arctic winter flights have provided information on chlorine partitioning for perturbed chemistry in the vortex. Stratospheric OH has been measured at 2.5 THz from a balloon instrument that is a precursor for satellite.

<insert Figure 10 near here>

Satellite-based Observations

Satellite-based observations can provide global coverage on a daily basis. Instruments, however, cost more and require longer development time than for other platforms. Limb-sounding is used for chemistry observations because of its vertical resolution and long path length for observations of small concentrations. Low-orbit (~700 km altitude) satellites have an observation path tangent point ~3000 km from the instrument. Vertical resolution of ~3 km, for example, then requires an antenna having vertical dimension of ~1000 wavelengths. Optically-thin O_2 emission and spectral line shapes provide information on the atmospheric pressure level at which the instrument field-of-view is pointed.

The need for global measurements of ClO motivated initial development of a satellite microwave instrument for stratospheric chemistry. The Microwave Limb Sounder (MLS) - operating unchopped in bands around 63, 183 and 205 GHz - was developed to measure ClO, O_3 and H_2O from NASA's Upper Atmosphere Research Satellite (UARS) launched in 1991. A somewhat similar instrument, the Millimeter-wave Atmospheric Sounder (MAS) was flown on 3 Space Shuttle missions between 1992 and 1994. MLS results showed enhanced ClO filling the lower stratosphere polar winter vortices of both the Antarctic and Arctic. This finding was especially important for the Arctic, demonstrating the effectiveness of localized PSCs in activating chlorine throughout the vortex. Observed ozone loss during periods of enhanced ClO is generally consistent with that expected from the ClO amount. MLS found that enhanced ClO appears in the edge of the Antarctic vortex by late May or early June each year and that by late July or early August the chlorine depletion of ozone starts to dominate ozone increases by transport. HNO_3 has been measured, providing insights into PSC microphysical processes and quantifying denitrification (removal of nitrogen) differences between the Arctic and Antarctic. **Fig. 11** shows daily maps of temperature, HNO_3, ClO and O_3 for both polar regions. Latitudinal variation in upper stratospheric zonal mean ClO from MLS appears qualitatively consistent with that expected

from variations in CH_4. Global ClO variations over a 6-year period have been related to CH_4 variations, increases in total chlorine, and changes in lower stratospheric chemistry associated with the decrease of aerosol from the Mt. Pinatubo volcano. MLS and MAS ClO measurements agree to within ~0.1 ppbv where comparisons have been possible.

<insert Figure 11 near here>

MLS H_2O measurements led to discovery of the atmospheric 'tropical tape recorder' whereby H_2O entering the tropical stratosphere is imprinted with a signature (the corresponding H_2O *saturation* mixing ratio) of the seasonally-varying tropopause temperature. They showed that midlatitude interhemispheric H_2O differences are not strongly related to the Antarctic winter vortex dehydration. Information has been obtained on various types of atmospheric oscillations and waves that affect the distribution of chemical species. Upper tropospheric H_2O, key for understanding aspects of climate variability, has been measured. The vertical profile of stratospheric SO_2 injected into the stratosphere by the Pinatubo volcano was measured for up to 6 months after the eruption, and its decay rate shown to be consistent with that expected from reaction with OH. Stratospheric CH_3CN has been measured. Weak signals can require averaging of data taken over long periods, which is feasible from satellite as well as from ground. **Fig. 12** shows a weak H_2O_2 line measured by averaging MLS data taken over 38 days.

<insert Figure 12 near here>

A Swedish small satellite 'Odin' for time-sharing atmospheric and astronomical observations became operational in 2001. It has microwave radiometers in bands centered near 118, 495, 550, 557 and 570 GHz to measure stratospheric H_2O (and its minor isotopes $H_2{}^{17}O$, $H_2{}^{18}O$ and HDO), O_3, ClO, N_2O, HNO_3, CO, NO, HO_2, H_2O_2 and temperature. A next-generation MLS has been developed for launch as part of NASA's Earth Observing System. EOS MLS has radiometers in 5 broad bands centered near 118, 190, 240, 640 GHz and 2.5 THz to make measurements throughout the stratosphere and upper troposphere as shown in **Fig. 13**. Japan is currently developing an SIS-based instrument for the International Space Station to measure stratospheric O_3 (including its minor isotopes and excited vibrational states) ClO, BrO, $H^{35}Cl$, $H^{37}Cl$, HOCl, HO_2, H_2O_2, HNO_3, volcanic SO_2 and temperature in spectral bands near 626 and 650 GHz. Several groups are also studying concepts for later experiments.

<insert Figure 13 near here>

Further Reading

deZafra, R. L. (1995) The Ground-Based Measurement of Stratospheric Trace Gases using Quantitative Millimeter Wave Emission Spectroscopy. Pages 23-54 in *Proc. of the International School of Physics "Enrico Fermi"*, Course CXXIV, G. Fiocco and G. Vicsonti, editors. Amsterdam: IOS Press.

Froidevaux, L., et al. (2000) Variations in the free chlorine content of the stratosphere (1991-1997): Anthropogenic, volcanic and methane influences. *J. Geophys. Res. 105*, pp 4471-4481.

Janssen, M. A., editor (1993) *Atmospheric Remote Sensing by Microwave Radiometry*. New York: John Wiley (chapter 8 has derivations of Equations [3] and [7], plots of spectra for most stratospheric species, and a more extensive version of Table 1).

Jarnot, R.F, et al. (1996) Calibration of the Microwave Limb Sounder on the Upper Atmosphere Research Satellite. *J. Geophys. Res. 101*, pp 9957-9982 (has a derivation of Equation [2]).

Mackenzie, I., et al. (1996) Chemical loss of polar vortex ozone inferred from UARS MLS measurements of ClO during the Arctic and Antarctic springs of 1993. *J. Geophys. Res. 101*, pp 14,505-14,518.

Manney, G.L., et al. (1994) Chemical depletion of ozone in the Arctic lower stratosphere during winter 1992-93. *Nature 370*, pp 429-434.

Mote, P.W., et al. (1996) An atmospheric tape recorder: the imprint of tropical tropopause temperatures on stratospheric water vapor. *J. Geophys. Res. 101*, pp 3989-4006.

Parrish, A., et al. (1981) Chlorine Oxide in the Stratospheric Ozone Layer: Ground Based Detection and Measurement. *Science 211*, pp 1158-1161.

Pickett, H. M., et al. (1998) Submillimeter, Millimeter, and Microwave Spectral Line Catalog. *J. Quantitative Spectroscopy and Radiative Transfer 60*, pp 883-890.

Read, W.G., et al. (2001) UARS MLS Upper Tropospheric Humidity Measurement: Method and Validation. *J. Geophys. Res. 106* , pp 32,207-32,258.

Rodgers, C.D. (2000) *Inverse Methods for Atmospheric Sounding*. Singapore: World Scientific Publishing Company Series on Atmospheric, Oceanic and Planetary Physics - Vol. 2.

Sandor, B.J. and Clancy, R.T. (1998) Mesospheric HO_x Chemistry from Diurnal Microwave Observations of HO_2, O_3, and H_2O. *J. Geophys. Res. 103*, pp 13,337-13,352.

Santee, M.L., et al. (1995) Interhemispheric differences in polar stratospheric HNO_3, H_2O, ClO and O_3. *Science 267*, pp 849-852.

Solomon, P.M., et al. (1987) High Concentrations of Chlorine Monoxide at Low Altitudes in the Antarctic Spring Stratosphere: Secular Variation. *Nature 328*, pp 411-413.

Waters, J. W., et al. (1993) Stratospheric ClO and ozone from the Microwave Limb Sounder on the Upper Atmosphere Research Satellite. *Nature 362*, pp 597-602.

Wu, D.L., and Waters, J.W. (1997) Observations of gravity waves with the UARS Microwave Limb Sounder. Pages 103-120 in *Gravity Wave Processes and Their Parameterization in Global Climate Models.* K. Hamilton, editor. New York: Springer-Verlag NATO ASI Series, vol. 50.

Table 1

Stratospheric species in decreasing order of the microwave 'figure of merit' $M = f\mu^2/Q$, where f is abundance in volume mixing ratio (column 5), μ is the dipole moment (column 3, where 1 Debye = 10^{-18} esu cm = 3.34×10^{-30} C m), and Q is the spin-rotation partition function (column 4, for a typical stratospheric temperature of 225 K). Excited vibrational states, indicated in parentheses (e.g., $2\nu_2$ indicates the second excited state of the second vibrational mode), are treated as separate species. The right column indicates if a microwave spectral line from that species has been detected by instruments from ground 'G', aircraft 'A', balloon 'B', or satellite 'S'. '(S)' indicates a satellite instrument to measure this molecule is planned for the near future. Species having $\log_{10}(M) \geq -15$ are included here. (Updated from Waters, J.W. (1993) Microwave Limb Sounding. ch. 8 in *Atmospheric Remote Sensing by Microwave Radiometry*. Janssen, M.A. ed., New York: John Wiley; Spectroscopic data from 9 Oct 2001 revision of the JPL Submillimeter, Millimeter, and Microwave Spectral Line Catalog, available on the world wide web at http://spec.jpl.nasa.gov.)

species	$\log_{10}(M)$	dipole moment (Debye)	partition function at 225 K	~maximum stratospheric abundance	has been microwave detected from
O_2	-6.4	0.0186	1.64×10^{2}	2.1×10^{-1}	G,A,B,S
H_2O	-6.8	1.847	1.16×10^{2}	5.0×10^{-6}	G,A,B,S
O_3	-8.9	0.5324	2.23×10^{3}	1.0×10^{-5}	G,A,B,S
^{18}OO	-9.1	0.0186	3.46×10^{2}	8.6×10^{-4}	G,(S)
HF	-9.4	1.827	7.96	1.0×10^{-9}	
$H_2{}^{18}O$	-9.5	1.855	1.17×10^{2}	1.0×10^{-8}	G,(S)
$H_2{}^{17}O$	-10.3	1.855	1.17×10^{2}	1.9×10^{-9}	(S)
HDO	-10.3	1.732	9.56×10^{1}	1.5×10^{-9}	G,(S)
HCl	-10.4	1.109	6.34×10^{1}	2.3×10^{-9}	A,B,(S)
^{17}OO	-10.6	0.0186	2.02×10^{3}	1.5×10^{-4}	
OH	-10.6	1.655	6.03×10^{1}	5.0×10^{-10}	A,B,(S)
$O_2(\nu_1)$	-10.7	0.0186	1.64×10^{2}	1.0×10^{-5}	
N_2O	-10.7	0.1608	3.74×10^{2}	3.0×10^{-7}	G,A,B,(S)
$H^{37}Cl$	-10.8	1.109	6.34×10^{1}	7.5×10^{-10}	A, B
$O_3(\nu_2)$	-10.9	0.5324	2.23×10^{3}	1.0×10^{-7}	G,B,(S)
$O_2(^1\Delta)$	-11.0	0.0186	1.13×10^{2}	3.0×10^{-6}	G
CO	-11.1	0.1101	8.17×10^{1}	5.0×10^{-8}	G,A,(S)
SO_2	-11.2 (a)	1.633	3.84×10^{3}	1.0×10^{-8} (a)	A,S(a)
HCN	-11.3	2.984	3.18×10^{2}	2.0×10^{-10}	G,(S)
^{16}O	-11.3	0.0186	6.324	1.0×10^{-7}	
$H_2O(\nu_2)$	-11.3	1.816	1.16×10^{2}	1.9×10^{-10}	
HNO_3	-11.5	1.986	1.82×10^{4}	1.5×10^{-8}	G,A,B,S
^{18}OOO	-11.6	0.5324	4.69×10^{3}	4.0×10^{-8}	G,B,(S)
$O^{18}OO$	-11.6	0.5324	2.29×10^{3}	2.0×10^{-8}	G
$O_3(\nu_3)$	-11.8	0.5324	2.23×10^{3}	1.3×10^{-8}	G,(S)

Table 1 (continued)

species	$\log_{10}(M)$	dipole moment (Debye)	partition function at 225 K	~maximum stratospheric abundance	has been microwave detected from
$O_3(\nu_1)$	-12.0	0.532	2.23×10^{3}	9.0×10^{-9}	G
^{35}ClO	-12.0	1.298	2.31×10^{3}	1.5×10^{-9}	G,A,B,S
$N_2O(\nu_2)$	-12.3	0.1608	3.74×10^{2}	7.0×10^{-9}	
^{37}ClO	-12.5	1.297	2.35×10^{3}	5.0×10^{-10}	
NO	-12.5	0.1587	8.17×10^{2}	1.0×10^{-8}	G(b),(S)
H_2CO	-12.5	2.331	1.87×10^{3}	1.0×10^{-10}	G
HO_2	-12.6	1.541	2.84×10^{3}	3.0×10^{-10}	G,A,B,(S)
OCS	-12.7	0.715	7.72×10^{2}	3.0×10^{-10}	
$O_3(2\nu_2)$	-12.8	0.5324	2.23×10^{3}	1.3×10^{-9}	
$HCN(\nu_2)$	12.8	2.942	1.06×10^{2}	2.0×10^{-12}	
NO_2	-12.9	0.316	8.76×10^{3}	1.0×10^{-8}	G
$HD^{18}O$	-13.0	1.726	9.68×10^{1}	3.0×10^{-12}	
$HNO_3(\nu_7)$	-13.1	1.986	1.82×10^{4}	3.8×10^{-10}	
^{13}CO	-13.1	0.1105	8.55×10^{1}	5.0×10^{-10}	
$O^{17}OO$	-13.1	0.5337	1.35×10^{4}	3.8×10^{-9}	(S)
^{17}OOO	-13.1	0.5337	2.73×10^{4}	7.6×10^{-9}	(S)
$N^{15}NO$	-13.1	0.1608	3.74×10^{2}	1.1×10^{-9}	
^{15}NNO	-13.1	0.1608	3.87×10^{2}	1.1×10^{-9}	
$HNO_3(\nu_9)$	-13.2	1.986	4.57×10^{4}	8.1×10^{-10}	
$H^{13}CN$	-13.2	2.984	3.27×10^{2}	2.2×10^{-12}	
$HC^{15}N$	-13.2	2.984	1.09×10^{2}	7.3×10^{-13}	
CH_3Cl	-13.2	1.899	1.83×10^{4}	3.0×10^{-10}	
$HNO_3(\nu_6)$	-13.3	1.986	1.82×10^{4}	2.4×10^{-10}	
^{18}OH	-13.3	1.667	6.06×10^{1}	1.0×10^{-12}	
H_2O_2	-13.4	1.572	5.76×10^{3}	1.0×10^{-10}	S
$N_2{}^{18}O$	-13.4	0.1608	3.96×10^{2}	6.0×10^{-10}	
DF	-13.5	1.819	1.48×10^{1}	1.5×10^{-13}	
CH_3CN	-13.5	3.922	2.36×10^{4}	5.0×10^{-11}	S
$O^{18}OO(\nu_2)$	-13.5	0.5324	2.45×10^{3}	2.2×10^{-10}	
$^{18}OOO(\nu_2)$	-13.6	0.5324	4.99×10^{3}	4.4×10^{-10}	
$HNO_3(\nu_8)$	-13.6	1.986	1.82×10^{4}	1.2×10^{-10}	
$O_3(\nu_2+\nu_3)$	-13.7	0.5324	2.23×10^{3}	1.6×10^{-10}	
$CH_3{}^{37}Cl$	-13.7	1.895	1.86×10^{4}	1.0×10^{-10}	
$HD^{17}O$	-13.8	1.73	9.6×10^{1}	5.7×10^{-13}	
$HO^{35}Cl$	-13.8	1.471	6.18×10^{3}	5.0×10^{-11}	(S)
$H^{81}Br$	-13.8	0.828	7.84×10^{1}	2.0×10^{-12}	
$H^{79}Br$	-13.8	0.828	7.84×10^{1}	2.0×10^{-12}	
$C^{18}O$	-13.8	0.1108	8.58×10^{1}	1.0×10^{-10}	
$O_3(\nu_1+\nu_2)$	-13.9	0.532	2.23×10^{3}	1.0×10^{-10}	
$N_2O(2\nu_2)$	-13.9	0.1608	3.74×10^{2}	1.7×10^{-10}	

Table 1 (continued)

species	$\log_{10}(M)$	dipole moment (Debye)	partition function at 225 K	~maximum stratospheric abundance	has been microwave detected from
^{18}O	-14.0	0.0186	6.324	2.0×10^{-10}	
$H^{15}NO_3$	-14.0	1.9	1.8×10^{4}	5.5×10^{-11}	
HO_2NO_2	-14.0	1.288	8.66×10^{4}	5.0×10^{-10}	
$O^{35}ClO$	-14.0	1.792	3.49×10^{4}	1.0×10^{-10}	
$OC^{34}S$	-14.1	0.715	7.78×10^{2}	1.2×10^{-11}	
$N_2{}^{17}O$	-14.1	0.16	3.8×10^{2}	1.1×10^{-10}	
^{79}BrO	-14.1	1.780	2.93×10^{3}	7.0×10^{-12}	
^{81}BrO	-14.1	1.780	2.94×10^{3}	7.0×10^{-12}	A,(S)
$HO^{37}Cl$	-14.2	1.471	6.29×10^{3}	2.0×10^{-11}	
$HDO(\nu_2)$	-14.2	1.7	9.5×10^{1}	2.0×10^{-13}	
$N_2O(\nu_1)$	-14.2	0.16	3.8×10^{2}	8.0×10^{-11}	
H_2SO_4	-14.4	2.725	1.01×10^{5}	5.0×10^{-11}	
$H_2{}^{13}CO$	-14.5	2.331	1.93×10^{3}	1.1×10^{-12}	
$O^{37}ClO$	-14.5	1.792	3.54×10^{4}	3.3×10^{-11}	
DCl	-14.5	1.103	1.18×10^{2}	3.0×10^{-13}	
$C^{17}O$	-14.6	0.1103	8.38×10^{1}	1.9×10^{-11}	
COF_2	-14.6	0.951	3.99×10^{4}	1.0×10^{-10}	
$O^{13}CS$	-14.7	0.715	7.74×10^{2}	3.3×10^{-12}	
^{17}O	-14.7	0.0186	6.324	3.8×10^{-11}	
$^{35}ClOO^{35}Cl$	-14.7	0.72	2.77×10^{5}	1.0×10^{-9}	
$OC^{18}O$	-14.8	0.0007	4.2×10^{2}	1.4×10^{-6}	
$^{35}ClONO_2$	-14.9	0.72	3.72×10^{5}	1.0×10^{-9}	

(a) Abundance and measurements are for enhanced SO_2 injected into the stratosphere by a volcanic eruption. Background SO_2 abundance in the stratosphere is $\sim10^{-11}$, corresponding to $\log_{10}(M) = -15.5$.

(b) The 250 GHz spectral line due to thermospheric NO has been measured.

Figures

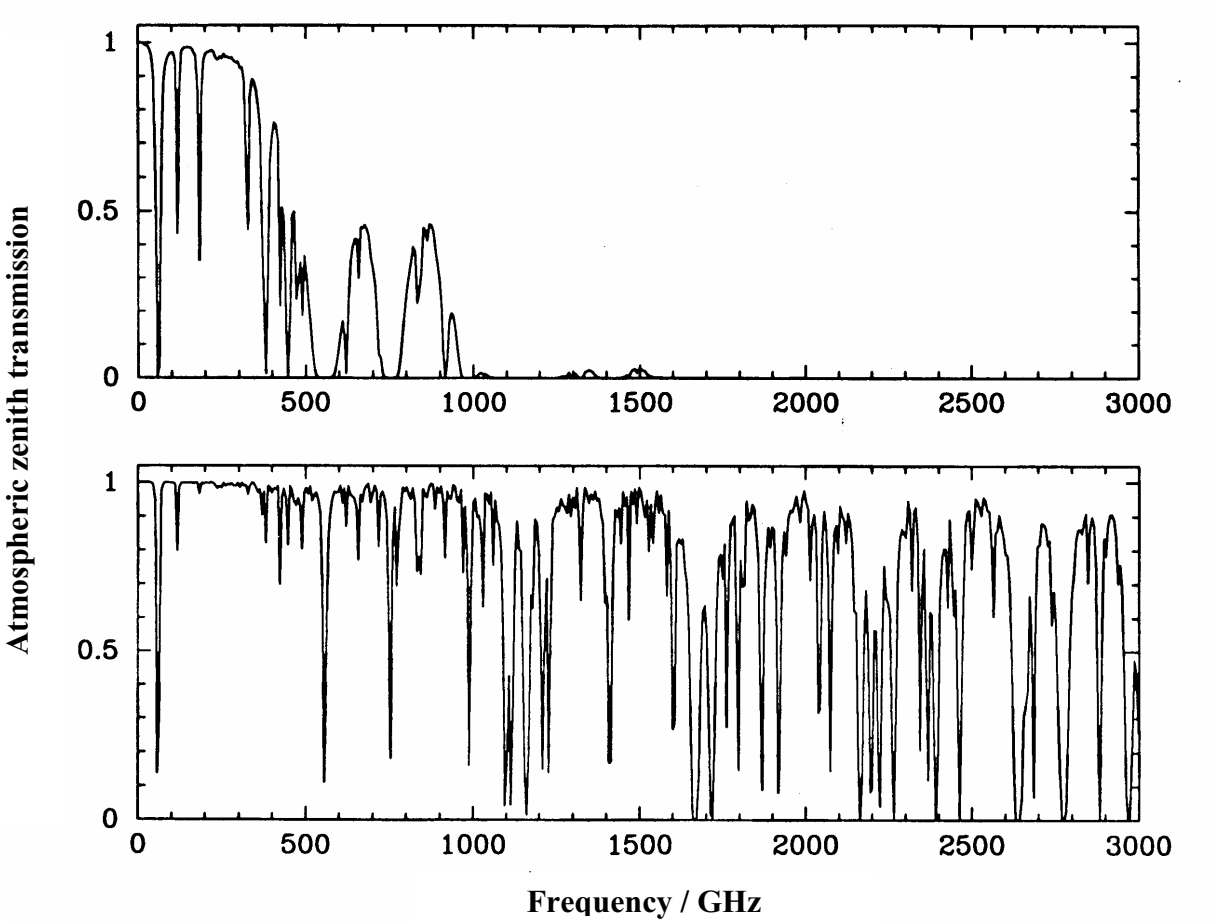

Figure 1 Atmospheric zenith transmission above a 4 km high mountain (top) and above an aircraft at 12 km (bottom). The absorption features seen here are due to H_2O and, to a lesser extent, O_2. (From Phillips, T. G., and Keene, J. (1992) Submillimeter Astronomy. *Proceedings of the IEEE 80*, pp 1662-1678. © 1992 Institute of Electrical and Electronics Engineers, Inc.)

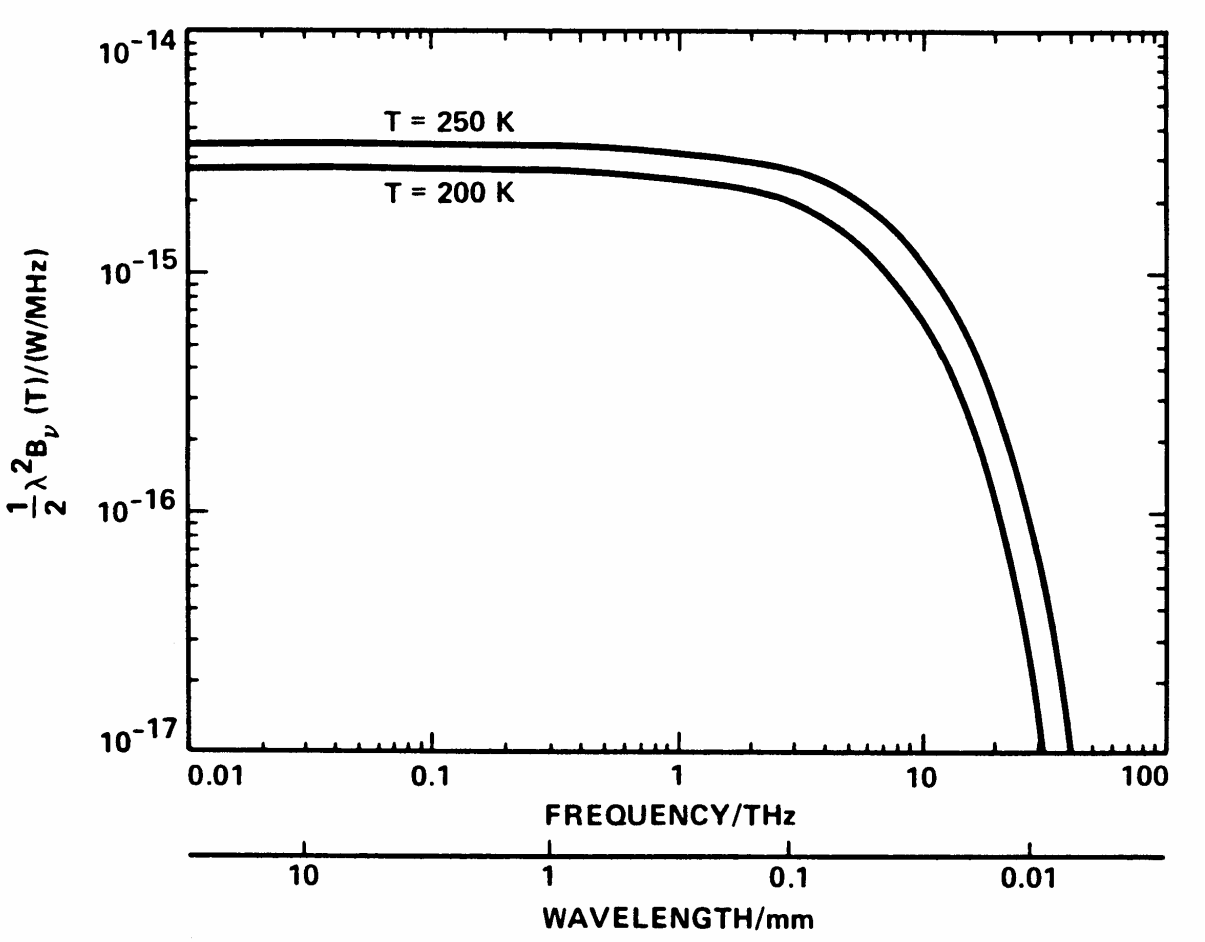

Figure 2 The power per unit frequency interval collected by a heterodyne instrument at frequency ν from a blackbody radiation field at 200 and 250 K. The function is plotted in units of W / MHz [1 MHz = 10^6 Hz], as MHz is the typical unit for widths of microwave spectral lines. (From Waters, J.W. (1993) Microwave Limb Sounding. chapter 8 in *Atmospheric Remote Sensing by Microwave Radiometry*. M.A. Janssen, ed. New York: John Wiley. © 1993 Wiley)

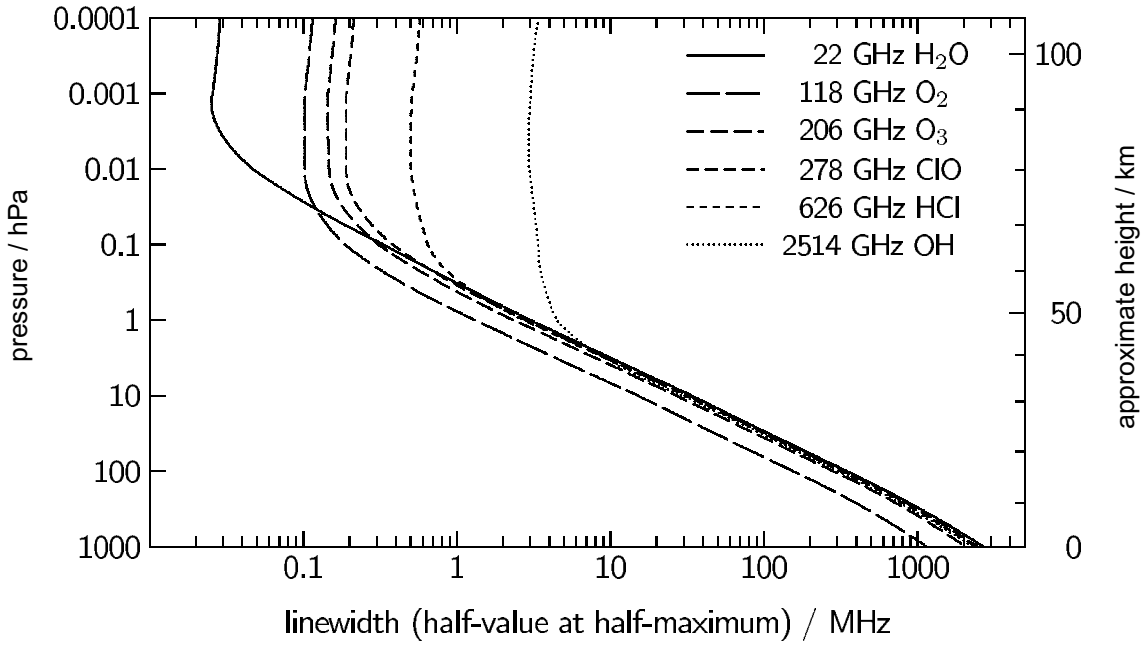

Figure 3 Linewidth (halfwidth at half maximum) versus altitude for some representative microwave spectral lines.

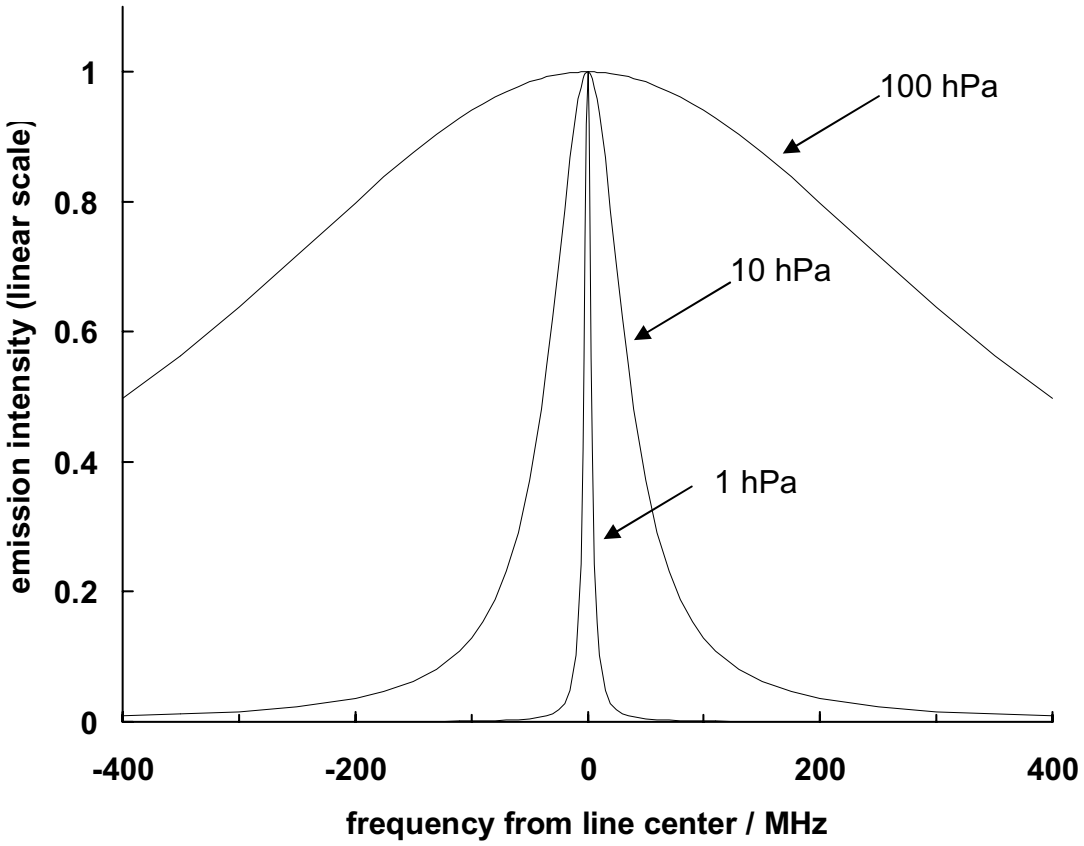

Figure 4 Microwave emission lines for the same mixing ratio of a gas at the bottom (100 hPa, ~15 km), middle (10 hPa, ~30 km), and top (1 hPa, ~50 km) of the stratosphere.

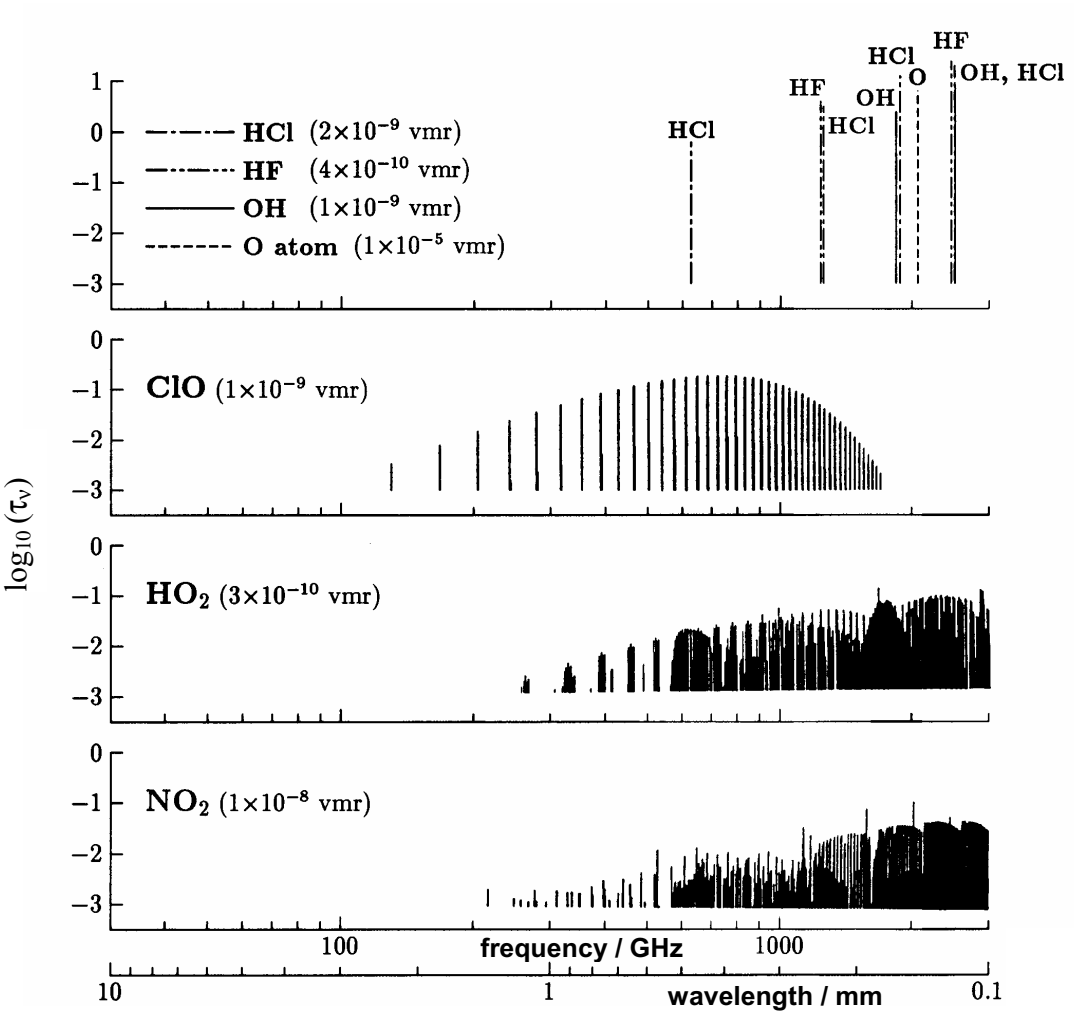

Figure 5 Spectra of some stratospheric molecules and atomic oxygen. Vertical axis is the logarithm of the optical depth for an observation path through the atmospheric limb with the indicated volume mixing ratios (vmr). (From Waters, J.W. (1993) Microwave Limb Sounding. chapter 8 in *Atmospheric Remote Sensing by Microwave Radiometry*. Janssen, M.A. ed. New York: John Wiley. © 1993 Wiley)

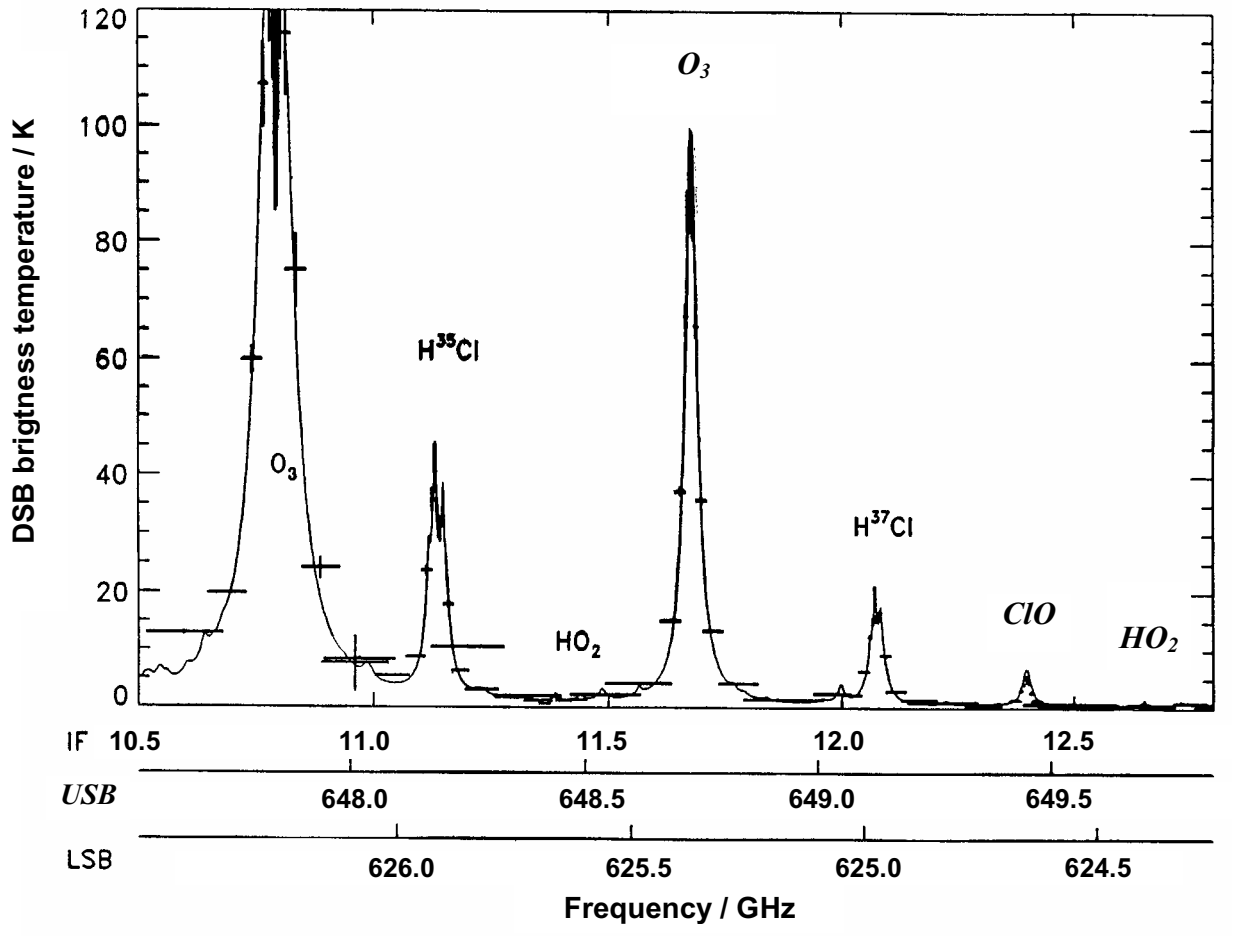

Figure 6 Measured (crosses, bars) and calculated (thin line) stratospheric emission spectrum in bands measured simultaneously near 626 and 649 GHz. 'USB' refers to the frequency covered by the upper sideband of the radiometer, 'LSB' to the lower sideband, and 'IF' to the intermediate frequency (see discussion in 'Instrumentation' section of text). LSB spectral lines are in sans serif font (e.g., $\mathsf{HO_2}$); USB lines are in italicized roman font (e.g., $\boldsymbol{HO_2}$). (Adapted from Stachnik, R.A., et al. (1992) Submillimeterwave Heterodyne Measurements of Stratospheric ClO, HCl, O_3 and HO_2: First Results. *Geophys. Res. Lett. 19*, 1931-1934.)

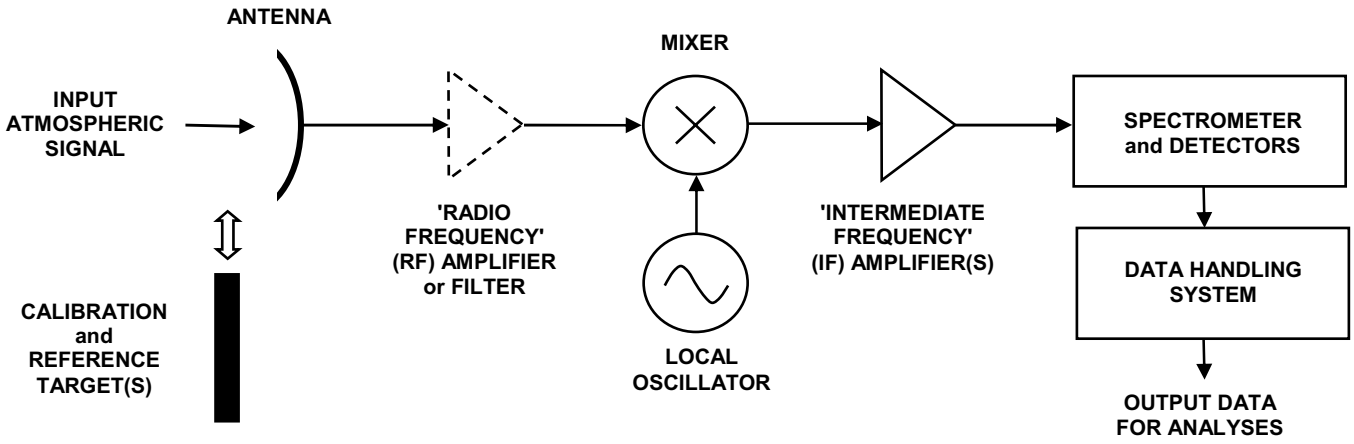

Figure 7 Typical block diagram of an instrument for microwave observations of stratospheric chemistry. The 'radio frequency' amplifier is currently available only at lower frequencies and does not appear in many systems; a filter is sometimes placed at this position to eliminate unwanted signals in one of the mixer's sidebands. The portion of the instrument between the antenna and spectrometer is called the 'receiver' or 'radiometer'.

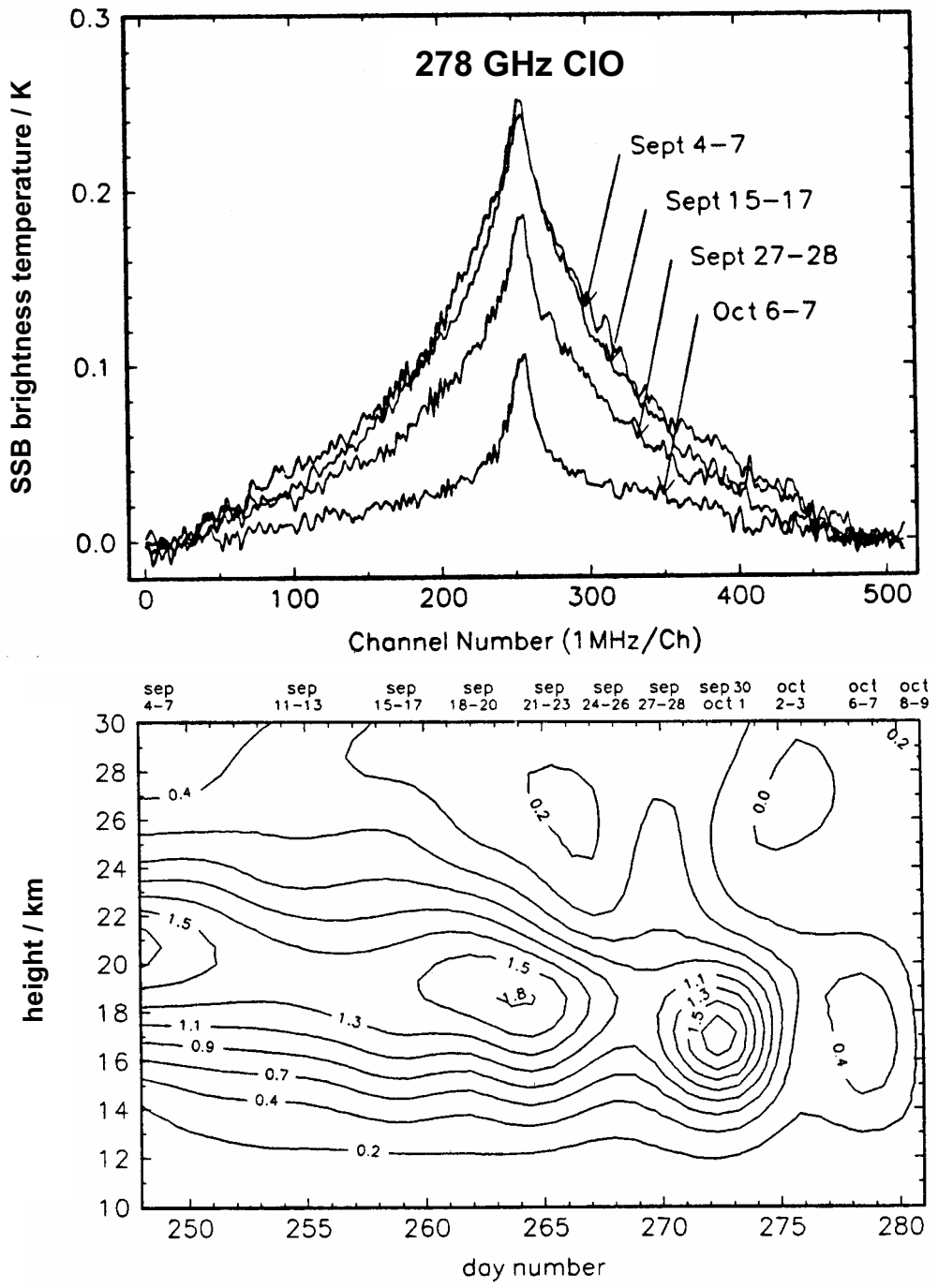

Figure 8 Ground-based 278 GHz measurement of stratospheric ClO over Antarctica. ClO is the key chlorine radical involved in ozone destruction. The top panel shows day-night differences of the spectral line measured during several days in 1992. The bottom panel shows a height-time cross section of the retrieved ClO mixing ratio profile, where contours are in parts per billion by volume. (From deZafra, R.L., Reeves, J.M., and Shindell, D.T. (1995) Chlorine monoxide in the Antarctic spring vortex 1. Evolution of midday vertical profiles over McMurdo Station, 1993. *J. Geophys. Res. 100*, pp 13,999-14,007. © 1995 American Geophysical Union)

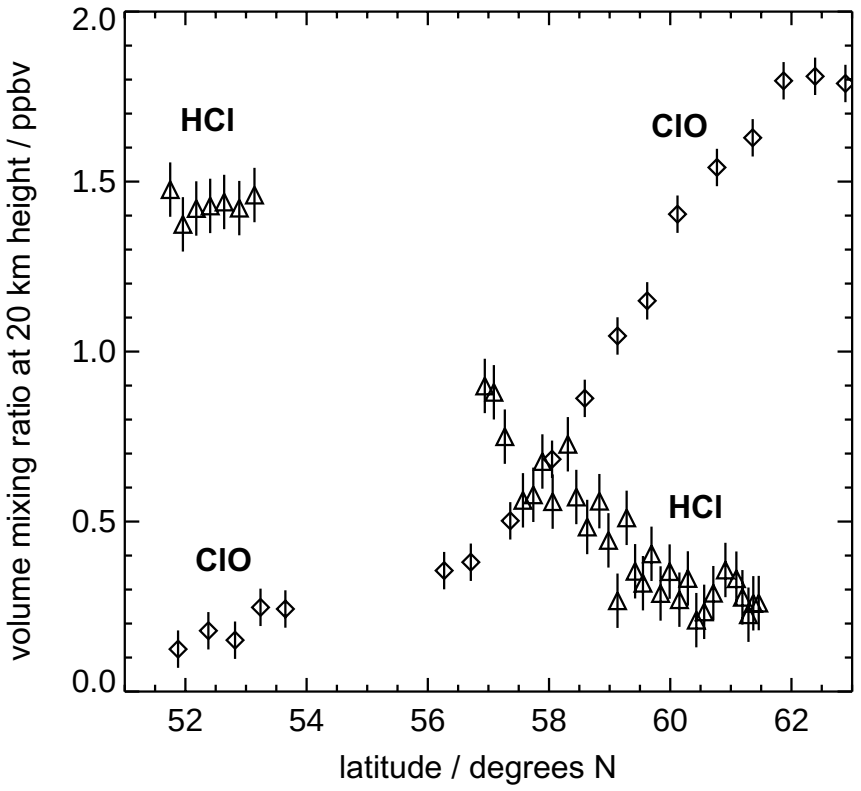

Figure 9 Aircraft measurements of stratospheric HCl (triangles, from the 626 GHz line) and ClO (diamonds, from the 649 GHz line) from a January 2000 flight through the edge of the Arctic vortex. Measurement time for each point is ~ 1 minute for HCl and ~ 3 minutes for ClO. These results show the transition of stratospheric chlorine from the relatively-inert HCl at lower latitudes to the highly-reactive ClO at higher latitudes inside the vortex. Gaps in the measurements around 54-56 N are where the instrument was tuned to measure HNO_3 and N_2O. (The instrument and campaign in which these measurements were made are described by Bremer, H., et al. (2002) Ozone depletion observed by ASUR during the Arctic Winter 1999/2000. *J. Geophys. Res. 107*, pp nnnn-nnnn. **[Note to editor: this paper currently in press; page numbers to be added later.]**)

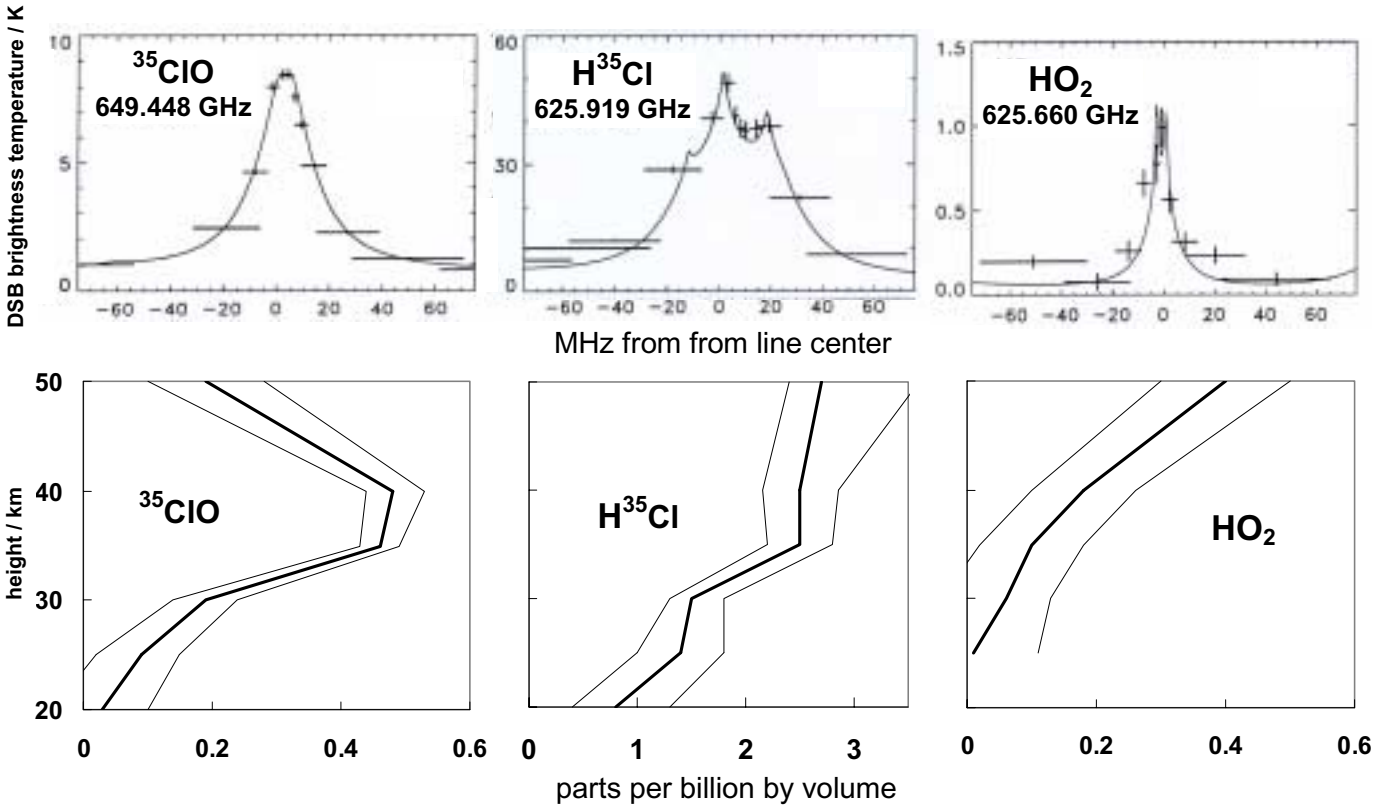

Figure 10 Balloon microwave measurements of ClO, HCl and HO_2. Top panels show the spectral lines for a limb observation path through the middle stratosphere: measurements are the horizontal bars whose widths give the spectral resolution of individual filters and smooth lines are calculated. Fine structure features are seen in the HCl line. The bottom panels show retrieved mixing ratio profiles (thick) and uncertainty limits (thin): (Adapted from Stachnik, R.A., et al. (1992) Submillimeterwave Heterodyne Measurements of Stratospheric ClO, HCl, O_3 and HO_2: First Results. *Geophys. Res. Lett. 19*, 1931-1934)

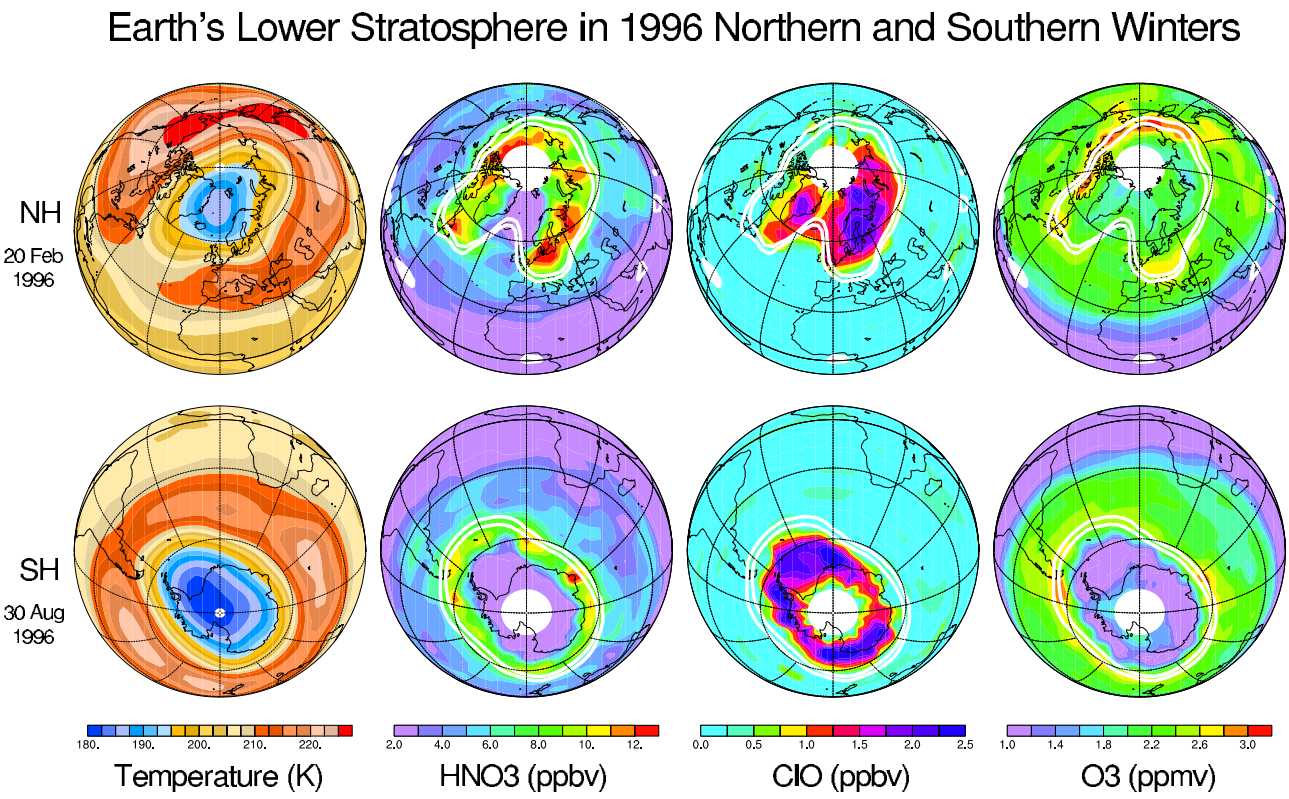

Figure 11 Earth's lower stratosphere in the Northern Hemisphere on 20 February 1996 (top) and in the Southern Hemisphere on 30 August 1996 (bottom). White contours show the dynamical edge of the polar vortices. HNO_3, ClO and O_3 are from the Microwave Limb Sounder on the Upper Atmosphere Research Satellite (no measurements are made in the white areas near the poles due to orbit limitations). Temperature data are from operational analyses of the U.S. National Center for Environmental Prediction. Temperatures in the blue and violet color ranges allow formation of polar stratospheric clouds from HNO_3 and H_2O; heterogeneous chemistry on these clouds leads to enhanced ClO that causes chemical depletion of O_3. HNO_3 also provides a source of NO_x , which quenches ClO and reduces the amount of ozone destruction. Both HNO_3 and O_3 increase in the lower stratospheric vortices during early winter due to downward transport of air rich in these species. The amount of ozone destruction each winter in the polar vortices depends on the duration of enhanced ClO, which is longer for the Antarctic than the Arctic. This difference is traceable to the Antarctic lower stratosphere being colder, and remaining cold for longer, than the Arctic. (From Waters J.W., et al. (1999) The UARS and EOS Microwave Limb Sounder Experiments. *J. Atmos. Sciences 56*, pp 194-218. © 1999 American Meteorological Society)

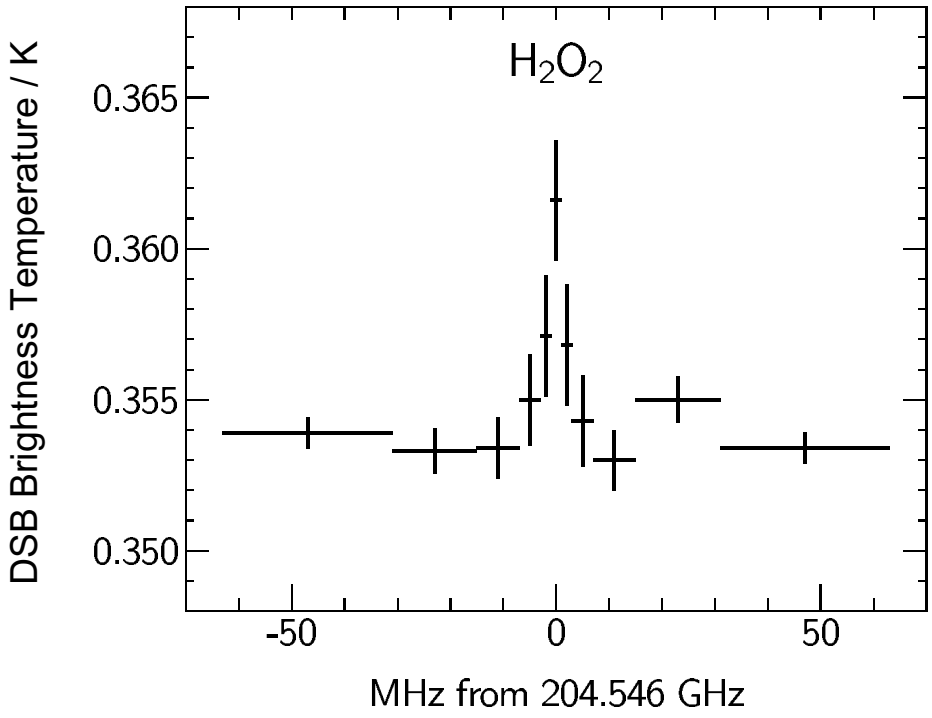

Figure 12 The weak 204 GHz H_2O_2 line from satellite measurements made over a period of 38 days, selected for tangent point pressure between 1 and 0.3 hPa (~2 days averaging time for the results shown here). Horizontal bars give the spectral resolution of individual filters and vertical bars give the $\pm 1\ \Delta T_{rms}$ measurement uncertainty calculated from Equation [9] for T_{rec}=1000 K DSB of the unchopped satellite instrument. The line strength corresponds to ~10^{-10} H_2O_2 volume mixing ratio in the upper stratosphere and lower mesosphere. The 0.353 K background is emission from the lower atmosphere received through the antenna sidelobes.

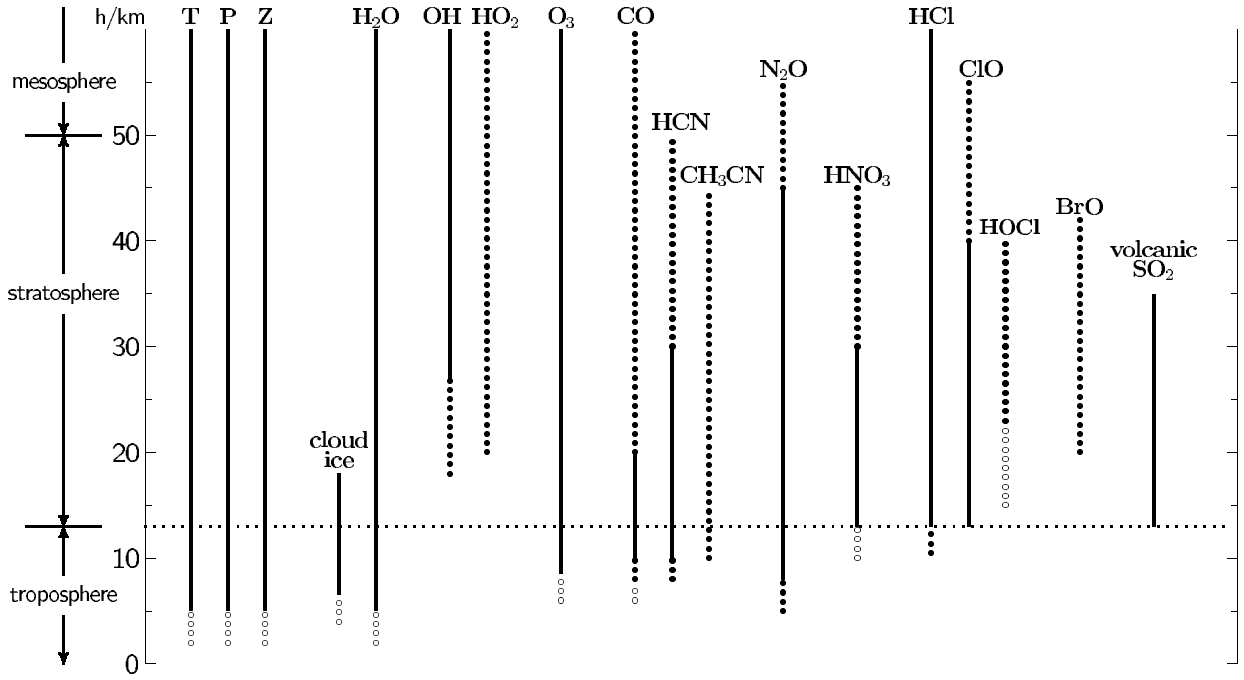

Figure 13 Measurements planned for the Earth Observing System Microwave Limb Sounder scheduled to begin operations in 2003 on NASA's 'Aura' satellite. P is pressure and Z is geopotential height. P, Z, H_2O, O_3, HCl, OH and CO measurements extend higher than the 60 km shown here. Closed circles indicate where averages will likely be required, and open circles at lowest altitudes are goals for more difficult measurements. (Updated from Waters, J.W., et al. (1999) The UARS and EOS Microwave Limb Sounder Experiments. *J. Atmos. Sciences 56*, 194-218.)